Large synthesis of in situ field measurements of the size distribution of mineral dust aerosols across their lifecycle

Paola Formenti[1] and Claudia Di Biagio[1]

[1] Université Paris Cité and Université Paris Est Creteil, CNRS, LISA, F−75013 Paris, France

Corresponding author : Paola Formenti (paola.formenti@lisa.ipsl.fr) and Claudia Di Biagio (claudia.dibiagio@lisa.ipsl.fr)

Abstract

Mineral dust aerosol is important in the Earth system and the correct representation of its size distribution is fundamental for shaping the current state and the evolution of climate. Despite many observational dust size data that are available in the literature, using this body of information to properly guide the development and validation of climate models and remote sensing retrievals remains challenging. In this study we collect, evaluate, harmonize, and synthetize 58 size distribution data from the past 50 years of in situ field observations with the aim of providing a consistent dataset to the community to use for constraining the representation of dust size across its lifecycle. Four levels (LEV) of data treatment are defined, going from original data (LEV0), data interpolated and normalized on a standardized diameter grid (LEV1), and data in which original particle diameters are converted into a common geometrical definition under both spherical (LEV2a) and aspherical (LEV2b) assumptions. Size distributions are classified as emission/source (SOURCE, <1 day from emission; number of datasets in this category, N=12), mid−range transport (MRT, 1−4 days of transport; N=36) and long−range transport (LRT, >4 days of transport; N=10). The harmonized dataset shows consistent features suggesting the conservation of airborne particles with time and a decrease of the main coarse mode diameter from a value of the order of 10 µm (in volume) for SOURCE dust to a value of the order of 1-2 µm for LRT conditions. An additional mode becomes evident below 0.4 µm for MRT and LRT dust. Data for the three levels (LEV1, LEV2a, LEV2b) and the three categories (SOURCE, MRT, LRT), together with statistical metrics (mean, median, 25% and 75% percentiles, and standard deviation) are made available as:

SOURCE (https://doi.org/10.57932/58dbe908-9394-4504-9099-74a3e77140e9; Formenti and Di Biagio, 2023a);

MRT (https://doi.org/10.57932/31f2adf7-74fb-48e8-a3ef-059f663c47f1; Formenti and Di Biagio, 2023b);

LRT (https://doi.org/10.57932/17dc781c-3e9d-4908-85b5-5c99e68e8f79; Formenti and Di Biagio, 2023c).

Introduction

Airborne mineral dust aerosols emitted by the aeolian erosion of bare soils contribute in a major way to the Earth's radiative budget and environmental processes, including the human health. Because of their native mineralogical composition and size distribution, they interact with solar and infrared radiation, influence the formation and brightness of liquid and ice clouds, and affect the composition of the atmosphere and the ocean, while also transporting pollutants, viruses and bacteria across the continents and the oceans (Knippertz and Stuut, 2014, and the many references therein).

As a consequence, a large effort has started in the last decades to include the representation of those properties in climate and air quality models. Indeed, the complex mineralogy of mineral dust, depending on that of the parent soils (Claquin et al., 1999; Journet et al., 2014; Gonçalves Ageitos et al., 2023a), is now accounted for in models (Scanza et al., 2015; Perlwitz et al., 2015a; 2015b; Menut et al., 2020; Kok et al., 2017; Di Biagio et al., 2020; Gómez Maqueo Anaya et al., 2024) and starts to be retrieved by remote sensing (Green et al., 2020; Zhou et al., 2020; Di Biagio et al., 2023).

On the other hand, representing the span and the variability in time and space of the dust aerosol size distribution remains a challenge.

The particle size distribution of mineral dust extends over several orders of magnitudes. Iron–rich particles as small as 14 nm in diameter have been observed in the laboratory from deflating soils by Baddock et al. (2013). During sandstorm in Algeria, Gomes et al. (1990) measured an increase of the mass concentration of particles between 100 nm and 1 µm, and attributed this to clays disaggregated by sandblasting. Measurements of the size–resolved vertical dust flux by Gillette et al. (1972; 1974a; 1974b) based on microscopy analyses of samples from Texas and Nebraska showed the presence of particles up to several microns in dust emissions.

The representation of the accumulation and coarse modes in mineral dust has long been based on the columnar measurements by the sun/sky photometers of the Aerosol Robotic Network (AERONET) network, which provides with normalized size distributions of mineral dust considered as chemically homogeneous particles the 0.1—30 µm optically–equivalent diameter (Dubovik et al., 2002; 2006; Holben et al., 2011), and which, incidentally, serve also the look–up tables of the remote sensing retrievals of dust from space (e.g., Cuesta et al., 2015; Zhou et al., 2020).

Nevertheless, in situ observations at ground–based stations and on aircraft in more recent years have shown that particles of several tens, sometimes hundreds, of micron are airborne at emission, and remain so after several days of transport (Reid et al., 2003; Formenti et al., 2003; Rajot et al., 2008; Chou et al., 2008; Kandler et al., 2007; 2009; Wagner et al., 2009; Klaver et al., 2011; Ryder et al., 2013; 2015; Rosenberg et al., 2014; Denjean et al., 2016; Wienzerl et al., 2017; van der Does et al., 2018).

These observations have been instrumental to a number of advances. Using them as ensemble dataset, to smooth local atmospheric variability, they have served as a basis to a new classification of the dust size distribution in four modes, namely fine dust (diameter ≤ 2.5 µm), coarse dust (2.5 < diameter ≤ 10 µm), super coarse dust (10 < diameter ≤ 62.5 µm) and giant dust (diameter > 62.5 µm), extending above the size range retrieved by AERONET (Adeyemi et al., 2023). Additionally, they have also fostered the revision of the numerical schemes of emissions and deposition, and identified the numerous processes and properties (non–spherical shape of particles, electric forces, atmospheric turbulence), that could counteract the size–selective removal by gravitational settling and keep particles airborne longer than expected (Kok, 2011; Huneeus et al., 2011; Mahowald et al., 2011; Kok et al., 2017; Di Biagio et al, 2020; Zhao et al., 2022; Adebiyi and Kok, 2020; Adebiyi et al., 2020; Huang et al., 2021; Meng et al., 2022; Adeyemi et al., 2023).

In support of those activities, in this paper we present a large and standardized compilation of *in situ* observations of the particle size distribution of mineral dust conducted during the past 50 years of research. This dataset extends the currently published compilations of measurements (Meng et al., 2022; Adeyemi et al., 2020; 2023) to provide with a state–of–the art of the current knowledge in support to the development of models, and ground–based and satellite remote sensing. Analysis of this dataset may provide with an integrated view of the size distribution of dust particles across their life cycle to evaluate their impacts in the Earth/human system.

2. Methods

2.1 Constitution of the dataset

Data presented in this paper result from in situ ground–based and aircraft observations of airborne dust conducted during field campaigns during the past 50 years of dust research. Data from deposition samples (e.g., van der Does et al. 2018 or Varga 2021) are not considered in this analysis.

Only datasets being published and properly referenced in the open peer–reviewed literature were retained. We also privileged datasets for which the methodology of acquisition, calibration and data treatment was well described so that the data quality can be assessed. Finally, we search for data as much as possible representative of different source and transport regions of the world.

The observations contributing to the dataset are listed in Table S1 and the spelling of the acronyms of the field campaigns is reported in Text S1 in the supporting material. Data are geo−localized in Figure 1, where they are classified with respect to their time after emission. Geographical coordinates are reported in Table S2.

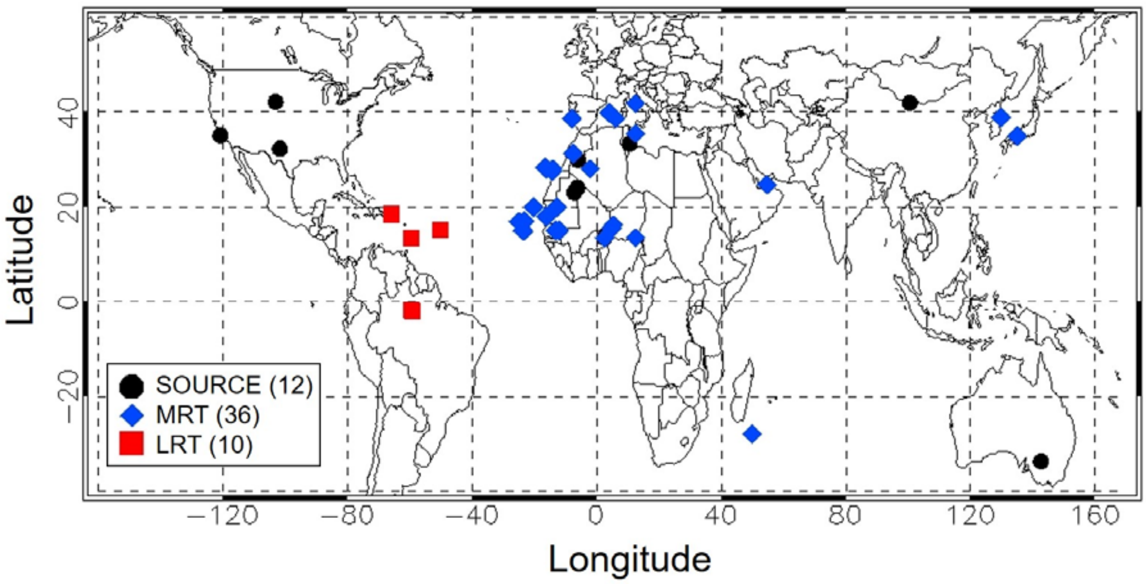

Figure 1. Geographical location of the datasets contributing to size distribution observations for the source, the mid−range transport (MRT) and the long−range transport (LRT) categories. The legend indicates the line style used in the plot. The number of data for each category is indicated in the parenthesis in the legend.

Observations obtained at the time of dust emission or within 1 day after emission are classified as SOURCE. Observations corresponding to 1 to 4 days after emission and/or geographically acquired near–source regions (for example, offshore North Africa) are classified as mid−range transport (MRT). Observations at times exceeding 4 days after emission or geographically distant from source regions (for example, observations in the Caribbean) are classified as long−range transport (LRT). To note that potential uncertainties may arise in this classification, in particular for datasets lying at the boundaries of the SOURCE, MRT and LRT categories, and we acknowledge this aspect as a source of error in our analysis. We invite the reader to refer to the Supplementary material (Text S4) for thorough description of the assumptions made in some cases to associate each dataset to a category.

The SOURCE dataset (Fig 1, black points) consists in 12 observations in Northern Africa, North America, and Asia, and one data set in Australia. They include works by Gillette et al. (1972, 1974), Gillette (1974), Fratini et al. (2007), Rajot et al. (2008), Sow et al. (2009), Shao et al. (2011), Ryder et al. (2013a, 2013b), Rosenberg et al. (2014), Huang et al. (2019), and Khalfallah et al. (2020), a set of data recently used by Kok et al. (2017), Di Biagio et al. (2020) and Huang et al. (2021) to constrain the shape of dust size distribution at emission in model studies, and the most recent work by Gonzales–Florez et al. (2023). The MRT class (Fig. 1, blue points) is contributed by 36 datasets from field campaigns (ACE2, ACE–Asia, ADRIMED, AER–D, AMMA, DABEX, DARPO, DIAPASON, DODO1–2, FENNEC, GAMARF, GERBILS, INDOEX, NAMMA, RHaMBLe, SALTRACE, SAMUM1–2, TRACE−P, and UAE2) in Western Africa, Capo Verde, the Mediterranean basin, the eastern tropical Atlantic, Saudi Arabia, Japan, and Indian Ocean, downwind sources either over the ocean or over desert areas. Additional datasets from studies performed in the

Sahara, the Atlantic Ocean, Canary Islands and Japan (Schütz, 1981; D'Almeida et al., 1987; Maring et al., 2000; Kobayashi et al., 2007) are added to the dataset. The LRT class (Fig. 1, red points) lays on 10 datasets of observations across the Atlantic Ocean and South America and is contributed by observations from Bacex, CLAIRE, Dust−Attack, Go−Amazon, PRIDE, and SALTRACE campaigns and intercontinental dust transport data from Schütz (1981).

2.2. Instrumentation contributing to the in situ dataset

The natural dynamical range of the particle size and concentration of mineral dust can only be represented by a combination of instruments based on different intrinsic particle properties such as density, electrical charge, shape and composition (e.g., Reid et al., 2003a; Formenti et al., 2011; Wendisch and Brenguier, 2013; Mahowald et al., 2014, Adeyemi et al., 2023). As a consequence, the datasets considered in this paper are contributed by different in situ instruments, also described in Text S2 in the supporting material, namely:

- Optical particle counters (OPC) using the dependence of light scattering on particle size and providing with the particle concentration as a function of the optical equivalent diameter (e.g., Reid et al., 2003b; Clarke et al., 2004; Osborne et al., 2008; Formenti et al., 2011; Ryder et al., 2013a, 2018; Khalfallah et al., 2020).
- Particle collection by filtration or impaction followed by individual particle characterization by transmission (TEM) and/or scanning electron microscopy (SEM) sizing particles as function of their equivalent projected−area diameter and coulter geometric sizing methods, (e.g., Gillette et al., 1972, 1974a, 1974b; Reid et al., 2003a; Khobayashi et al., 2007; Kandler et al., 2009; Chou et al., 2008).
- Multi−stage filtration or impaction sampling coupled with gravimetric or chemical analysis providing with the mass size distribution as equivalent aerodynamic diameter (e.g., Formenti et al., 2001; Reid et al., 2003b).
- Differential and Scanning Mobility Particle Sizer (DMPS and SMPS) providing the size of particles in the submicron range as the electrical mobility equivalent diameter of a charged particle moving in a static electric field (e.g., Maring et al., 2000, 2003; Bates et al., 2002; Müller et al., 2010; Denjean et al., 2016a, 2016b).
- Aerodynamic particle sizers (APS), measuring the equivalent aerodynamic diameter of a sphere of unit density having the same terminal velocity in an accelerated airflow as the irregularly shaped dust particles (e.g., Maring et al., 2003; Reid et al., 2003b; 2008; Struckmeier et al., 2016)

Each of those instrument types size particles on an equivalent diameter (optical, projected−area, aerodynamic, mobility) that depends on their respective working principle. Converting those operational size definitions into a homogenized one is part of the treatment applied in this work, which follows the theory proposed and discussed in the literature and benefits of recent progresses in characterizing/synthetizing dust properties relevant for these treatments (e.g., Hinds, 1999, De Carlo et al., 2004 ; Mahowald et al., 2014; Di Biagio et al., 2019; Huang et al., 2020, 2021; Formenti et al., 2021). Diameter definitions and formulas to convert each of them into a geometrical diameter, both under the assumption of spherical and aspherical dust, is provided in Text S3 and summarized in Table S3.

Text S4 presents relevant information on each dataset considered in the present analysis. This includes a brief description of the field operations, the experimental conditions, the type of original data (number, volume or mass concentration size distribution, size−resolved emission fluxes), the instrumentation, and the data treatment applied to the measurements (averages, diameter corrections, etc.) in the original publication. Original data were obtained, as much as possible, through a personal contact with the data providers or from the original publications. This is also indicated in Text S4.

2.3. Data treatment, harmonization, and synthesis

The original observations were treated to provide with a harmonized dataset in terms of the definition of particle diameter and data were normalized to remove differences in sampled number concentrations. Four level of data treatment are defined as described below.

1/ *Level−0 (LEV0)*: original data, taken at the native resolution or the resolution from digitalization process and converted into volume distribution assuming spherical particles ($\pi/6*D^3*dN/d\log D$), where *D* is the particle diameter used in the publication and d*N*/dlogD is the particle number concentration. To remove differences in concentration, and in absence of information on original bin width, *LEV0* data are normalized to the maximum of the volume size distribution;

2/ *Level−1 (LEV1)*: data from *LEV0* are interpolated over a common size range of equi−logarithmically spaced diameters (dlog*D* = 0.05) encompassing the original diameter range for each dataset and normalized so that the integral is equal to 1 over a common diameter range. The diameter range for integral normalization was set to be the largest as possible and to be covered by more than 90% of the datasets in each category. For SOURCE data it resulted that the diameter range for common integral normalization is within 1.58 and 7.1 µm, and for MRT and LRT it is between 0.71 and 8.9 µm.

3/ *Level−2a (LEV2a)*: based on *LEV1*, the *LEV2a* data treatment aims at harmonizing the size distributions by converting the operational original particle diameters, which depend on the physical principle of each instrument, into a common−defined sphere−equivalent geometric diameter. Data from LEV1 are treated as in the following with respect to their diameter corrections:

- data already provided as geometrical diameters (from coulter counters, i.e., only one dataset in our study) are left unchanged;
- data provided as projected−area diameters (i.e. from microscopy) are left unchanged;
- data provided as aerodynamic diameters (from APS or cascade impactors) are corrected assuming a shape factor (χ) of 1 (under spherical assumption), therefore a size−invariant conversion factor of 1.58 (see Eq. S2) is applied to the dataset assuming dust density of 2.5 g cm^{-3} ($D_{geom}=D_{aerod}/1.58$). If original aerodynamic diameter data are already converted into geometrical diameter, we replace the original correction with the conversion factor of 1.58. Since the correction is a multiplicative factor the dlogD of the bins remain unchanged;
- data provided as optical diameters (from OPCs) are converted into sphere−equivalent geometric diameters applying the optical to geometrical correction by assuming homogeneous spherical particles and a value of CRI of 1.53−0.003i. This CRI value is at the average of the dust refractive indices reported in the 370-950 nm spectral range in Di Biagio et al. 2019) for dust of global origin. Data for applying the correction for the different model of OPCs considered were taken from Formenti et al. (2021) and conversion factors were recalculated at the dlogD path of 0.05 assumed in the interpolated sizes. For the GRIMM 1.108 for which calibration is not provided in Formenti et al. (2021) we used the data taken from Formenti et al. (2011) interpolated at the 0.05 dlogD path of our diameters. In order to avoid discontinuities appearing and because of the new dlogD do not significantly differ on average from the value of 0.05 for D_{geom} calculated from D_{opt} interpolated data, we do not update the dlogD, so that the conversion only imply a shift of the diameter. More details on the choices applied for corrections in different cases are provided in Text S4. Original datasets already converted into geometrical diameter, are left unchanged. However, it is worth noting that the ensemble of data already applying an optical to geometrical correction uses a CRI varying between 1.53 and 1.55 for the real part and 0.001 and 0.004 for the imaginary part and work under the hypothesis of homogeneous spherical particles (Mie theory), therefore consistent with our treatment. Exceptions are Khalfallah et al. (2020) using a CRI of 1.43−0.00i as for quartz particles, and González–Flórez et al. (2023) using a CRI of 1.49–0.0015i and also applying calculations in ellipsoidal assumption instead of Mie theory. The only dataset not theoretically submitted to the optical to geometric correction is the one provided by Renard et al. (2018) using an OPC built with a specific geometry making the measurements very low sensitive to CRI calibration.

4/ *Level−2b (LEV2b)*: based on LEV1, the LEV2b data treatment aims at harmonizing the size distributions by converting the operational original particle diameters into a common–defined geometrical diameter by taking into account that mineral dust is aspherical. Data from LEV1 are treated as in the following with respect to their diameter corrections:

- data already provided as geometrical diameters from coulter counters are left unchanged. This technique is in fact only slightly affected by shape effects, as discussed by Kobayashi et al. (2007);
- data provided as projected−area diameters are corrected using the size−invariant correction factor of 1.56 from Huang et al. (2021) ($D_{geom}=D_{area}/1.56$) (see Eq. S1);
- data provided as aerodynamic diameter are corrected assuming a size−invariant conversion factor of 1.45 following Huang et al. (2021) ($D_{geom}=D_{aerod}/1.45$) (see Eq. S2);
- data provided as optical diameters and already treated as for LEV2a data, are further corrected by applying a size−dependent aspherical to spherical ratio ($ASR(D_{geom})$) correction function, $ASR(D_{geom})=(D_{geom})_{aspherical}/(D_{geom})_{spherical}$, to take into account non–sphericity effects in optical to geometrical conversion. The ASR function (Fig. S1) is obtained by combining the optical to geometrical diameter conversion factors for different OPCs calculated by Formenti et al. (2021) and Huang et al. (2021) both in the assumption of spherical homogeneous particles $(D_{geom})_{spherical}$ and tri−ellipsoids dust $(D_{geom})_{aspherical}$. More details are provided in Text S3. Original datasets derived from OPC measurements already provided as geometrical diameter but under assumption of sphericity are also corrected by applying the $ASR(D_{geom})$ converting function. The only exception are González–Flórez et al. (2023), that already apply tri–axial ellipsoids calculations in their optical to geometric conversion, and Renard et al. (2018), not requiring optical to geometrical conversion.

As for LEV1, the LEV2a and LEV2b data, for which a known interpolation path is used, are normalized so that the integral of the volume size distribution is 1 over a common diameter range (1.58 – 7.1 µm for SOURCE, 0.71 – 8.9 µm for MRT, LRT).

For each category (SOURCE, MRT, LRT) and for each data level (LEV1, LEV2a, LEV2b), the mean, median, and standard deviation of the particle volume concentration per size class are calculated where at least 2 datasets are available in the diameter range. Additionally, the 25% and 75% percentiles are also calculated, despite keeping in mind their limited representativeness given the reduced number of samples in the datasets, especially for SOURCE and LRT classes.

2.4. Limitations of the chosen approach

Some precisions should be given when considering the LEV2a and LEV2b treatment reported in this work. First, the implicit assumption when applying LEV2a and LEV2b dataset corrections is that dust is the dominant aerosol species and possible effects due to internal or external mixing of dust with other aerosol types are not taken into considerations (i.e., in the complex refractive index or shape factor assumptions). Second, for those datasets that are obtained from the combination of different techniques, namely DMPS+APS (Bates et al., 2002; Maring et al., 2000, 2003; Müller et al., 2010), OPC+APS (Chen et al., 2011), SMPS + OPC (de Reus et al., 2000; Otto et al;, 2007; Denjean et al., 2016a, 2016b), DMPS + APS + microscopy (Kandler et al., 2011), or multiple OPC instruments (Reid et al., 2003b; McConnell et al., 2008; Johnson and Osborne, 2011; Ryder et al., 2013a, 2013b, 2018; Rosenberg et al., 2014; Weinzierl et al., 2009, 2011, 2017), the choice is that of applying artefact corrections for the dominant instrument, often the one in the extended coarse mode range, and consider this correction applicable to the whole diameter range. This is because when multiples instruments are used to build a size distribution it is then not easy to reconstruct the steps of data analysis and merging from the original work. It follows the subsequent considerations:

1/ the corrections applied for the aerodynamic and projected−area diameter apply a constant size−invariant scaling factor to the ensemble of the size distribution data. In this approximation, if the SMPS/DMPS is combined with aerodynamic or microscopy data, a correction factor between

1.45 and 1.58, depending on the level and the technique as detailed in the previous section, is applied in place of the factor 1 (spherical assumption) or 1.19 (aspherical assumption) (see Eq. S3) expected to convert the mobility diameter to geometrical diameter in LEV2a and LEV2b data. As a consequence, the submicron size is 20 to 58% finer than expected only due to mobility to geometrical conversion.

2/ A similar approach is used to correct datasets where OPC is the main used technique to size dust particles together with the SMPS. For LEV2a data the Mie correction is applied to the full size distribution, but being the size−dependent correction mostly inactive for submicron particles (i.e. D_{geom} ~ D_{opt} for most OPCs), the approach is mostly equivalent at considering a mobility diameter correction with a shape factor of 1. For LEV2b data, using OPC corrections induce a limited right shifting of the size distribution compared to the one that would be obtained from mobility conversion because of the magnitude of the ASR function (Fig. S1) compared to the shape factor of 1.19 assumed for aspherical dust.

3/ When datasets relying on multiple OPCs measurements, the assumption is that the "dominant" OPC that is the OPC covering the largest range and the coarsest sizes in particular, is considered. Given that optical to geometrical corrections are not relevant for submicron particles and that the magnitude of the correction typically increases for increasing sizes, this assumption is not expected to determine significant biases in the data. To mention additionally a general ambiguity of the optical to geometrical correction around the diameter of 1 µm where a plateau in the scattering calibration function for several OPCs models can be found (i.e. Formenti et al., 2021).

More details on the specific assumptions and choices done for each dataset are provided in Text S4.

Further, for LEV2a and LEV2b data for which corrections are applied on the data, caution is taken at the boundary of the size distribution and when the first and/or the last bin of the corrected size showed significant divergence, these data are removed from the dataset.

An additional source of erroris the individual measurement uncertainty, which varies with the specific setup, instrument and spatial and temporal extent of the measurement.

3. Presentation and discussion of the dataset

Illustration of the data for different levels is provided in Figure 2. Figure 3 presents the synthesis of the LEV2b data and the comparison of SOURCE, MRT and LRT distributions. The contribution of different size classes to the total particle number, surface and volume is summarised in Table 1. Size classes have been defined according to the classification of Adeyemi et al. (2023) defining fine dust ($D \leq 2.5$ µm), coarse dust ($2.5 < D \leq 10$ µm), super coarse dust ($10 < D \leq 62.5$ µm) and giant dust ($D > 62.5$ µm). Within the fine dust class, we further calculate the fractions of particles smaller than 0.4 µm.

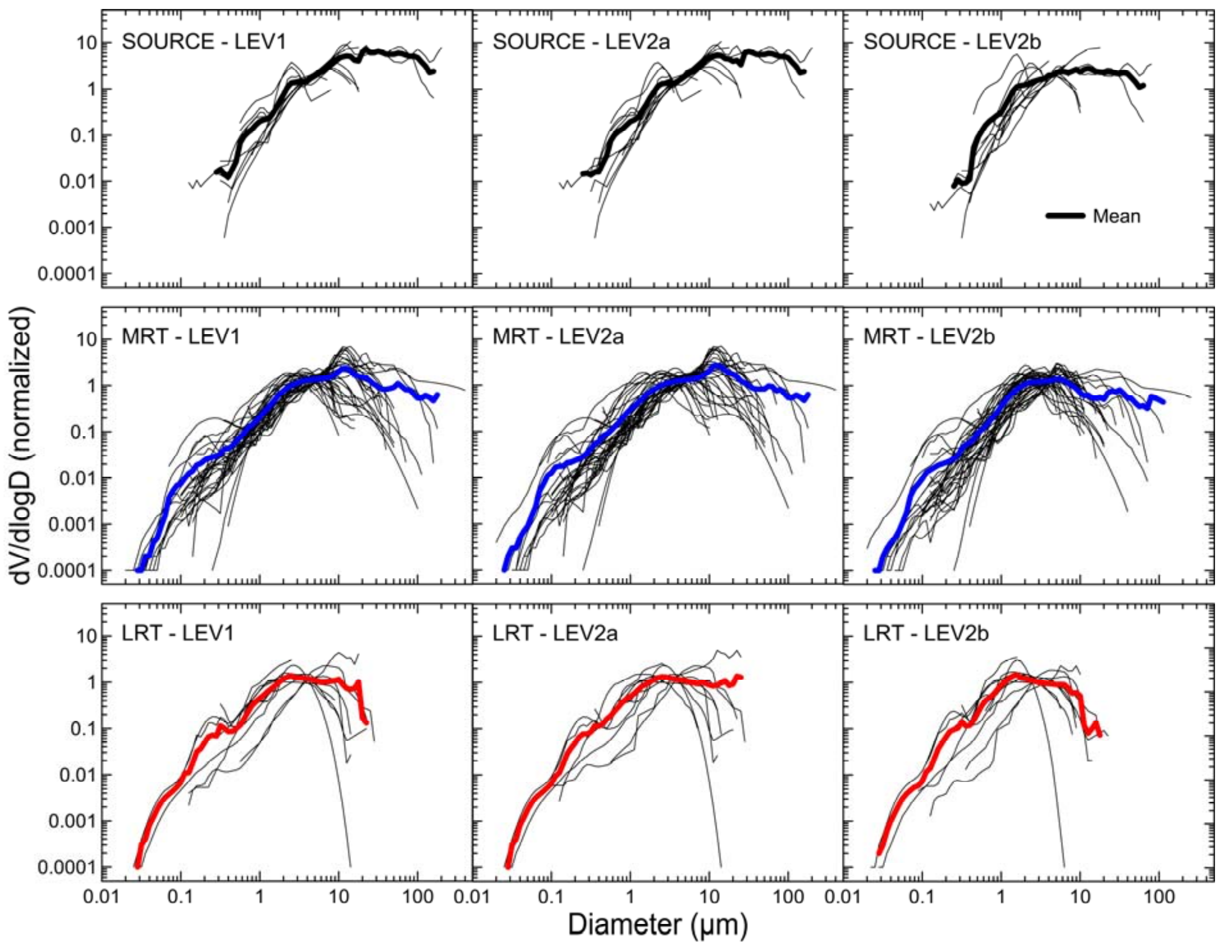

Figure 2. Data for SOURCE, MRT, and LRT dust at level 1, 2a, and 2b as described in Sect. 2.3 (labelled as LEV1, LEV2a, LEV2b, respectively). Single datasets, all normalized at the integral of 1, are plotted as black lines. The mean (thick black, blue, and red line for SOURCE, MRT, and LRT, respectively) are shown at all levels. Note that the mean is calculated only where at least 2 datasets are available in the diameter range.

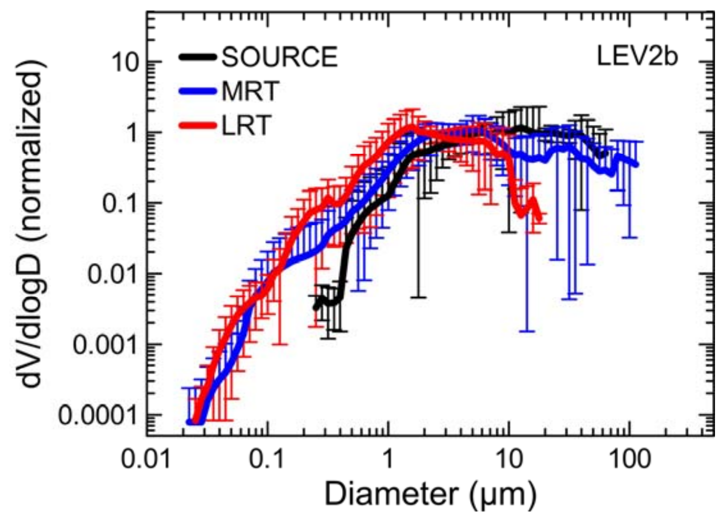

Figure 3. Comparison of normalized mean volume size distribution for the SOURCE, MRT, and LRT categories in our study reported as LEV2b data (mean ± standard deviation). For the sake of comparison, and differently from data in Fig. 2, the SOURCE, MRT, and LRT synthesis datasets reported here are normalized at the integral equal to 1 over a common diameter range corresponding to 0.35–17.8 μm. This is done to remove differences linked to different integration range for SOURCE data compared to MRT and LRT.

Dataset		D ≤ 2.5 µm (D ≤ 0.4 µm)	2.5 < D ≤ 10 µm	10 < D ≤ 62.5 µm	D > 62.5 µm
Number	SOURCE	95.4% (20.4%)	4.5%	0.1%	0.4%
	MRT	99.8% (96.1%)	0.2%	0.0%	0.0%
	LRT	99.9% (94.5%)	0.1%	0.0%	0.0%
Surface	SOURCE	45.0% (1.1%)	39.4%	15.5%	0.14%
	MRT	65.4% (16.8%)	30.7%	3.6%	0.29%
	LRT	84.6% (23.1%)	15.1%	0.2%	0.00%
Volume	SOURCE	10.8% (0.1%)	34.9%	52.7%	1.6%
	MRT	22.1% (1.1%)	44.3%	25.7%	8.0%
	LRT	53.4% (3.6%)	44.5%	2.0%	0.0%

Table 1. Percentages of number, surface and volume size distribution in the diameter ranges D ≤ 0.4 µm, D ≤ 2.5 µm, 2.5 < D ≤ 10 µm, 10 < D ≤ 62.5 µm, and D > 62.5 µm for the mean of the size obtained for the SOURCE, MRT, and LRT LEV2b datasets.

As shown in Fig. 2 and 3 the shape of the dust size distribution at emission and along transport shows main consistent features. A main mode located at ~10 µm (in volume) is observed for dust at emission and close to sources, as based from the few studies allowing to measure up to the coarse fraction. The main dust mode decreases to ~5 µm and ~2 µm for MRT and LRT conditions, respectively. Below 0.4 µm the dust volume size shows an additional mode, particularly visible for MRT and LRT. As a matter of fact, the sparse datasets measuring very fine particles at the SOURCE show that particles with diameters below 0.4 µm (however measured only down to 0.2 µm, as shown in Fig. 2) represent approximately 20% of the total particles' number, increasing to more than 90% in MRT and LRT. Instruments such as SMPS and DMPS used in MRT and LRT studies measure particles as small as 0.02 µm in diameter. Previous single–particle compositional observations showing that the particle number concentration in the size range between 0.1 and 0.4 µm is largely contributed by aluminosilicate dust particles at emission, while internal or external mixing with aerosols other than dust gains importance with time and altitude of transport (Chou et al., 2008; Kandler et al., 2007, 2009; Weinzierl et al., 2009; 2017; Klaver et al., 2011; Denjean et al., 2016a; 2016b).

The normalized size distribution of dust particles between 0.4 and 10 µm is rather consistent and invariant along the dust cycle. This is true in particular when restricting to the 2.5 to 10 µm size range when differences are minimal and contribution to total volume is in between 34.9% and 44.5%. Below that range, which is between 0.4 and 2.5 µm, the contribution of particles for LRT is significantly higher (53.4% in volume) than for SOURCE (10.8%) and MRT (22.1%), likely as, because of the normalization, it compensates the decrease of particles larger than 10 µm.

The magnitude of the particle volume above 10 µm remains unchanged almost up to 100 µm for both the SOURCE and the MRT conditions, which also present similar particle volume. This mode decreases very strongly for LRT conditions, when it represents only 2% of the total volume, compared to almost 55% and 34% for SOURCE and MRT, respectively.

The dataset presented in this work, synthetizing available *in situ* observations, allows evaluation of the natural variability of dust size distribution along its lifecycle. To be emphasized, however, that while consistent differences in the mean size distribution curves are obtained going from SOURCE to LRT, as shown in Fig. 3, the inherent range of variability for each category, represented by the standard deviation of the data, is also non–negligible and reflects the large range of documented size distributions, together with the limited statistics available. This is particularly true for both super–coarse and giant dust at MRT and LRT. Lower variability is identified below 0.4 µm because of the restricted number of dataset available for MRT and LRT conditions, and there is an absence of data for SOURCE dust below this size range.

Finally, to facilitate the use of these data within models and remote sensing schemes, Table 2 provides the parameters of lognormal size distributions fitting the LEV2a and LEV2b mean values of the three dust categories. Lognormal functions are set to reproduce the main shape of the dust distribution above 0.4 µm, neglecting the specific features below this diameter where information is lower and the size affected by particle mixing with other compounds, especially for MRT and LRT. We found that a single broad mode can be employed to represent the main features of the volume size distributions above 0.4 µm. Plots of the fitting functions are provided in supplementary Fig. S4. Because there is an inherent level of subjectivity in the choice of the number of modes and their parameters, we invite the individual researchers using the data to implement the parameterizations in accordance to their scientific needs.

Dataset	Lognormal mode				
	N_{tot} (# cm^{-3})	NMD (µm)	V_{tot} (nm^3 cm^{-3})	VMD (µm)	σ
SOURCE – LEV2a	5.08 10^{-10}	0.355	7.76	26.69	3.32
SOURCE – LEV 2b	9.8 10^{-10}	0.300	3.38	11.71	3.02
MRT – LEV 2a	2.11 10^{-9}	0.150	2.55	11.64	3.33
MRT – LEV 2b	6.82 10^{-9}	0.100	1.57	5.79	3.20
LRT – LEV 2a	2.35 10^{-9}	0.280	1.39	3.88	2.55
LRT – LEV 2b	2.96 10^{-9}	0.350	1.15	2.34	2.22

Table. *Parameters (total number and volume concentration, N_{tot} (# cm^{-3}),V_{tot} (nm^3 cm^{-3}), number and volume median diameter, NMD and VMD (µm), geometric standard deviation, σ) for the log-normal modes used to parameterize the LEV2b volume size distributions of the SOURCE, MRT, and LRT categories. Parameters refers to the following equations:* $\frac{dV}{dlogD} = \frac{\pi}{6} D^3 \frac{N_{tot}}{\sqrt{2\pi} log\sigma} exp\left(-\frac{(logD - logNMD)^2}{2(log\sigma)^2}\right)$ *and* $\frac{dV}{dlogD} = \frac{V_{tot}}{\sqrt{2\pi} log\sigma} exp\left(-\frac{(logD - logVMD)^2}{2(log\sigma)^2}\right)$

4. Conclusive remark

In this paper we present the most possible comprehensive synthesis of *in situ* observations of the particle size distribution of atmospheric dust aerosols. This compilation reflects the current state–of–the–art and represents a standardized and synthetic benchmark to constrain and evaluate models and satellite retrievals. We highlight differences and commonalities of the dust volume distribution as a function of time in the atmosphere, both in terms of main identified modes and relative contribution of dust in different size ranges.

We did this based on a large statistics of data and permit to retrieve robust information between 0.4 and 10 µm where most of observations exist, while above and below this size range, observations are rare. Dust particles below 0.4 µm in diameter are seldom measured close to source regions, but are found in observations at mid– and long–range transport conditions. Their presence at emission, their size–segregated composition and state of mixing should be better documented and understood. The dynamics of the coarse mode above 10 µm, its invariance from source to mid-range transport, and decline afterwards is reported, and can challenge models.

We acknowledge the evidence that the compilation of a reference dataset is, almost by definition, a subjective and incomplete exercise which must revised continuously with the emergence of new datasets, new field campaigns, and the improvement of sampling techniques. We henceforth encourage colleagues to provide us with new or revised datasets to feed and update the dataset in the future.

Data availability

The LEV1, LEV2a and LEV2b datasets discussed in this paper are available on the EaSy Data, the Earth System Data repository (https://www.easydata.earth/#/public/home, last access: 01 June 2024) maintained by the National French DATA TERRA research Infrastructure. Their respective DOIs are summarized here below:

SOURCE_LEV1.dat, SOURCE_LEV2a.dat, SOURCE_LEV2b.dat : https://doi.org/10.57932/58dbe908-9394-4504-9099-74a3e77140e9 (Formenti and Di Biagio, 2023a);

MRT_LEV1.dat, MRT_LEV2a.dat, MRT_LEV2b.dat: https://doi.org/10.57932/31f2adf7-74fb-48e8-a3ef-059f663c47f1 (Formenti and Di Biagio, 2023b);

LRT_LEV1.dat, LRT_LEV2a.dat, LRT_LEV2b.dat : https://doi.org/10.57932/17dc781c-3e9d-4908-85b5-5c99e68e8f79 (Formenti and Di Biagio, 2023c).

Figures of the individual datasets (including LEV0) are provided upon request.

Code availability. Data from images on published papers were digitalized with the online WebplotDigitizer software available at https://automeris.io/WebPlotDigitizer/

Author contributions. PF and CDB designed the research, compiled and analysed the dataset, and wrote the manuscript.

Competing interests. The authors declare that they have no competing interests.

Special issue statement. The paper is not associated with a special issue.

Acknowledgements

PF and CDB acknowledge J. L. Rajot, C. Denjean, A. Adeyemi, D. Meloni, C. Ryder, and J. Kok for providing the original data from their publications. The authors would like to thank G. Schuster (NASA/Langley), R. Miller (NASA/Giss) and the second anonymous referee for their effort in improving the paper and the data access. The help of G. Brissebrat (CNRS/DATA TERRA/Aeris), H. Bressan and S. Grellet (GaiaData BRGM) in creating the DOI for the different datasets and solving the access issues is gratefully acknowledged.

Funding

This research is funded by the project DustClim, part of ERA4CS, an ERA–NET initiated by JPI Climate, and funded by FORMAS (SE), DLR (DE), BMWFW (AT), IFD (DK), MINECO (ES), ANR (FR) with co–funding by the European Union (Grant 690462).

References

Adebiyi, A. A., and Kok, J. F.: Climate models miss most of the coarse dust in the atmosphere, Science Advances, 6, eaaz9507, doi:10.1126/sciadv.aaz9507, 2020.

Adebiyi, A. A., Kok, J. F., Wang, Y., Ito, A., Ridley, D. A., Nabat, P., and Zhao, C.: Dust Constraints from joint Observational–Modelling–experiMental analysis (DustCOMM): comparison with measurements and model simulations, Atmos. Chem. Phys., 20, 829–863, https://doi.org/10.5194/acp–20–829–2020, 2020.

Adebiyi, A. A., J. Kok, B. J Murray, C. L Ryder, J.-B. W. Stuut, R. A. Kahn, P. Knippertz, P. Formenti, N. M Mahowald, C. Pérez García-Pando, M. Klose, A. Ansmann, B. H. Samset, A. Ito, Y. Balkanski, C. Di Biagio, M. N. Romanias, Y. Huang, and J. Meng, A review of coarse mineral dust in the Earth system, Aeol. Res., 60, https://doi.org/10.1016/j.aeolia.2022.100849, 2023.

d'Almeida, G. A.: On the variability of desert aerosol radiative characteristics, J. Geophys. Res: Atmos., 92, 3017–3026, https://doi.org/10.1029/JD092iD03p03017, 1987.

d'Almeida, G. A. and Schütz, L.: Number, Mass and Volume Distributions of Mineral Aerosol and Soils of the Sahara, J. Climate Appl. Meteor., 22, 233–243, https://doi.org/10.1175/1520–0450(1983)022<0233:NMAVDO>2.0.CO;2, 1983.

Bates, T. S., Coffman, D. J., Covert, D. S., and Quinn, P. K.: Regional marine boundary layer aerosol size distributions in the Indian, Atlantic, and Pacific Oceans: A comparison of INDOEX measurements with ACE–1, ACE–2, and Aerosols99, J. Geophys. Res., 107, INX2 25–1–INX2 25–15, https://doi.org/10.1029/2001JD001174, 2002.

Baddock, M., Boskovic, L., Strong, C., McTainsh, G., Bullard, J., Agranovski, I., and Cropp, R.: Iron–rich nanoparticles formed by aeolian abrasion of desert dune sand, Geochemistry, Geophysics, Geosystems, 14, 3720–3729, https://doi.org/10.1002/ggge.20229, 2013.

Chen, G., Ziemba, L. D., Chu, D. A., Thornhill, K. L., Schuster, G. L., Winstead, E. L., Diskin, G. S., Ferrare, R. A., Burton, S. P., Ismail, S., Kooi, S. A., Omar, A. H., Slusher, D. L., Kleb, M. M., Reid, J. S., Twohy, C. H., Zhang, H., and Anderson, B. E.: Observations of Saharan dust microphysical and optical properties from the Eastern Atlantic during NAMMA airborne field campaign, J. Geophys. Res., 11, 723–740, https://doi.org/10.5194/acp–11–723–2011, 2011.

Chou, C., Formenti, P., Maille, M., Ausset, P., Helas, G., Harrison, M., and Osborne, S.: Size distribution, shape, and composition of mineral dust aerosols collected during the African Monsoon Multidisciplinary Analysis Special Observation Period 0: Dust and Biomass–Burning Experiment field campaign in Niger, J. Geophys. Res.,, 113, https://doi.org/10.1029/2008JD009897, 2008.

Claquin, T., Schulz, M., and Balkanski, Y.: Modeling the mineralogy of atmospheric dust sources, J. Geophys. Res., 104, 22243–22256, 1999.

Clarke, A. D., Shinozuka, Y., Kapustin, V. N., Howell, S., Huebert, B., Doherty, S., Anderson, T., Covert, D., Anderson, J., Hua, X., Moore, K. G., McNaughton, C., Carmichael, G., and Weber, R.: Size distributions and mixtures of dust and black carbon aerosol in Asian outflow: Physiochemistry and optical properties, J. Geophys. Res., 109, https://doi.org/10.1029/2003JD004378, 2004.

Cuesta, J., Maxim Eremenko, C. Flamant, Gaelle Dufour, Benoit Laurent, Gilles Bergametti, M. Hopfner, J. Orphal and D. Zhou, Three-dimensional distribution of a major desert dust outbreak over East Asia in March 2008 derived from IASI satellite observations, J. Geophys. Res., 120, 7099-7127, 2015

Denjean, C., Formenti, P., Desboeufs, K., Chevaillier, S., Triquet, S., Maillé, M., Cazaunau, M., Laurent, B., Mayol-Bracero, O. L., Vallejo, P., Quiñones, M., Gutierrez-Molina, I. E., Cassola, F., Prati, P., Andrews, E., and Ogren, J.: Size distribution and optical properties of African mineral dust after intercontinental transport, J. Geophys. Res., 121, 7117–7138, https://doi.org/10.1002/2016JD024783, 2016a.

Denjean, C., Cassola, F., Mazzino, A., Triquet, S., Chevaillier, S., Grand, N., Bourrianne, T., Momboisse, G., Sellegri, K., Schwarzenbock, A., Freney, E., Mallet, M., and Formenti, P.: Size distribution and optical properties of mineral dust aerosols transported in the western Mediterranean, Atmos. Chem. Phys., 16, 1081–1104, https://doi.org/10.5194/acp–16–1081–2016, 2016b.

Di Biagio, C., Formenti, P., Balkanski, Y., Caponi, L., Cazaunau, M., Pangui, E., Journet, E., Nowak, S., Andreae, M. O., Kandler, K., Saeed, T., Piketh, S., Seibert, D., Williams, E., and Doussin, J.-F.: Complex refractive indices and single-scattering albedo of global dust aerosols in the shortwave spectrum and relationship to size and iron content, Atmos. Chem. Phys., 19, 15503–15531, https://doi.org/10.5194/acp-19-15503-2019, 2019.

Di Biagio, C., Y. Balkanski, S. Albani, O. Boucher, and P. Formenti, Direct radiative effect by mineral dust aerosols constrained by new microphysical and spectral optical data, Geophys. Res. Lett., 47, e2019GL086186. https://doi.org/10.1029/2019GL086186, 2020.

Di Biagio, C., Doussin, J. F., Cazaunau, M., Pangui, E., Cuesta, J., Sellitto, P., Rodenas, M., and Formenti, P., Infrared optical signature reveals the source–dependency and along–transport evolution of dust mineralogy as shown by laboratory study, Sci. Rep., 13, 13252, https://doi.org/10.1038/s41598-023-39336-7, 2023.

Dubovik, O., B.N. Holben, T.F. Eck, A. Smirnov, Y.J. Kaufman, M.D. King, D. Tanre, and I. Slutsker (2002), Variability of absorption and optical properties of key aerosol types observed in worldwide locations, J. Atmos. Sci., 59, 590–608, doi:10.1175/1520-0469(2002)059<0590:VOA.

Dubovik, O., et al. (2006), Application of spheroid models to account for aerosol particle nonsphericity in remote sensing of desert dust, J. Geophys. Res., 111, D11208, doi:10.1029/2005JD006619.

Formenti, P., Andreae, M. O., Lange, L., Roberts, G., Cafmeyer, J., Rajta, I., Maenhaut, W., Holben, B. N., Artaxo, P., and Lelieveld, J.: Saharan dust in Brazil and Suriname during the Large–Scale Biosphere–Atmosphere Experiment in Amazonia (LBA) – Cooperative LBA Regional Experiment (CLAIRE) in March 1998, J. Geophys. Res., 106, 14919–14934, https://doi.org/10.1029/2000JD900827, 2001.

Formenti, P., Rajot, J. L., Desboeufs, K., Saïd, F., Grand, N., Chevaillier, S., and Schmechtig, C.: Airborne observations of mineral dust over western Africa in the summer Monsoon season: spatial and vertical variability of physico–chemical and optical properties, J. Geophys. Res., 11, 6387–6410, https://doi.org/10.5194/acp–11–6387–2011, 2011.

Formenti, P., Di Biagio, C., Huang, Y., Kok, J., Mallet, M. D., Boulanger, D., and Cazaunau, M.: Look–up tables resolved by complex refractive index to correct particle sizes measured by common research–grade optical particle counters, Atmos. Meas. Tech. Discuss. [preprint], https://doi.org/10.5194/amt–2021–403, in review, 2021.

Formenti P. and C Di Biagio, Large synthesis of in situ field measurements of the size distribution of mineral dust aerosols across their lifecycle-SOURCE. https://doi.org/10.57932/58dbe908-9394-4504-9099-74a3e77140e9, 2023a.

Formenti P. and C Di Biagio, Large synthesis of in situ field measurements of the size distribution of mineral dust aerosols across their lifecycle-MRT. https://doi.org/10.57932/31f2adf7-74fb-48e8-a3ef-059f663c47f1, 2023b.

Formenti P. and C Di Biagio, Large synthesis of in situ field measurements of the size distribution of mineral dust aerosols across their lifecycle-LRT https://doi.org/10.57932/17dc781c-3e9d-4908-85b5-5c99e68e8f79, 2023c.

Fratini, G., Ciccioli, P., Febo, A., Forgione, A., and Valentini, R.: Size–segregated fluxes of mineral dust from a desert area of northern China by eddy covariance, Atmos. Chem. Phys., 7, 2839–2854, https://doi.org/10.5194/acp–7–2839–2007, 2007.

Gillette, D. A., Blifford, I. H., and Fenster, C. R.: Measurements of Aerosol Size Distributions and Vertical Fluxes of Aerosols on Land Subject to Wind Erosion, J. Appl. Meteor., 11, 977–987, https://doi.org/10.1175/1520–0450(1972)011<0977:MOASDA>2.0.CO;2, 1972.

Gillette, D.A. On the production of soil wind erosion having the potential for long range transport, J. Rech. Atmos. 8, 734–744, 1974.

Gillette, D. A., Blifford, I. H., and Fryrear, D. W.: The influence of wind velocity on the size distributions of aerosols generated by the wind erosion of soils, J. Geophys. Res. 79, 4068–4075, https://doi.org/10.1029/JC079i027p04068, 1974.

Gomes, L., G. Bergametti, G. Coudé–Gaussen, and P. Rognon, Submicron Desert Dusts: A Sandblasting Process, J. Geophys. Res., 95 (D9), 927–940, 1990.

Gómez Maqueo Anaya, S., Althausen, D., Faust, M., Baars, H., Heinold, B., Hofer, J., Tegen, I., Ansmann, A., Engelmann, R., Skupin, A., Heese, B., and Schepanski, K.: The implementation of dust mineralogy in COSMO5.05-MUSCAT, Geosci. Model Dev., 17, 1271–1295, https://doi.org/10.5194/gmd-17-1271-2024, 2024.

González–Flórez, C., Klose, M., Alastuey, A., Dupont, S., Escribano, J., Etyemezian, V., Gonzalez–Romero, A., Huang, Y., Kandler, K., Nikolich, G., Panta, A., Querol, X., Reche, C., Yus–Díez, J., and Pérez García–Pando, C.: Insights into the size–resolved dust emission from field measurements in the Moroccan Sahara, Atmos. Chem. Phys., 23, 7177–7212, https://doi.org/10.5194/acp–23–7177–2023, 2023.

Gonçalves Ageitos, M., V. Obiso, R.L. Miller, O. Jorba, M. Klose, M. Dawson, Y. Balkanski, J. Perlwitz, S. Basart, E. Di Tomaso, J. Escribano, F. Macchia, G. Montané, N. Mahowald, R.O. Green, D.R. Thompson, and C. Pérez García–Pando, 2023: Modeling dust mineralogical composition: sensitivity to soil mineralogy atlases and their expected climate impacts, *Atmos. Chem. Phys.*, **23**, no. 15, 8623–8657, doi:10.5194/acp–23–8623–2023.

Green, R. O. *et al.* The earth surface mineral dust source investigation: an earth science imaging spectroscopy mission. in: *2020 IEEE Aerospace Conference* 1–15 (2020). https:// doi. org/ 10. 1109/ AERO4 7225. 2020. 91727 31.

Huang, Y., Kok, J. F., Martin, R. L., Swet, N., Katra, I., Gill, T. E., Reynolds, R. L., and Freire, L. S.: Fine dust emissions from active sands at coastal Oceano Dunes, California, 19, 2947–2964, https://doi.org/10.5194/acp–19–2947–2019, 2019.

Huang, Y., Adebiyi, A. A., Formenti, P., & Kok, J. F., Linking the different diameter types of aspherical desert dust indicates that models underestimate coarse dust emission. Geophys. Res. Lett., 48, e2020GL092054, https://doi.org/10.1029/2020GL092054, 2021.

Huneeus, N., Schulz, M., Balkanski, Y., Griesfeller, J., Prospero, J., Kinne, S., Bauer, S., Boucher, O., Chin, M., Dentener, F., Diehl, T., Easter, R., Fillmore, D., Ghan, S., Ginoux, P., Grini, A., Horowitz, L., Koch, D., Krol, M. C., Landing, W., Liu, X., Mahowald, N., Miller, R., Morcrette, J.-J., Myhre, G., Penner, J., Perlwitz, J., Stier, P., Takemura, T., and Zender, C. S.: Global dust model intercomparison in AeroCom phase I, Atmos. Chem. Phys., 11, 7781–7816, https://doi.org/10.5194/acp-11-7781-2011, 2011.

Johnson, B. T. and Osborne, S. R.: Physical and optical properties of mineral dust aerosol measured by aircraft during the GERBILS campaign, Q. J. Royal. Met. Soc., 137, 1117–1130, https://doi.org/10.1002/qj.777, 2011.

Journet, E., Balkanski, Y., and Harrison, S. P.: A new data set of soil mineralogy for dust-cycle modeling, Atmos. Chem. Phys., 14, 3801–3816, https://doi.org/10.5194/acp-14-3801-2014, 2014.

Jung, E., Albrecht, B., Prospero, J. M., Jonsson, H. H., and Kreidenweis, S. M.: Vertical structure of aerosols, temperature, and moisture associated with an intense African dust event observed over the eastern Caribbean, J. Geophys. Res., 118, 4623–4643, https://doi.org/10.1002/jgrd.50352, 2013.

Kaaden, N., Massling, A., Schladitz, A., Müller, T., Kandler, K., Schütz, L., Weinzierl, B., Petzold, A., Tesche, M., Leinert, S., Deutscher, C., Ebert, M., Weinbruch, S., and Wiedensohler, A.: State of mixing, shape factor, number size distribution, and hygroscopic growth of the Saharan anthropogenic and mineral dust aerosol at Tinfou, Morocco, Tellus B, 61, 51–63, https://doi.org/10.1111/j.1600–0889.2008.00388.x, 2009.

Kandler, K., SchüTZ, L., Deutscher, C., Ebert, M., Hofmann, H., JäCKEL, S., Jaenicke, R., Knippertz, P., Lieke, K., Massling, A., Petzold, A., Schladitz, A., Weinzierl, B., Wiedensohler, A., Zorn, S., and Weinbruch1, S.: Size distribution, mass concentration, chemical and mineralogical composition and derived optical parameters of the boundary layer aerosol at Tinfou, Morocco, during SAMUM 2006, Tellus B, 61, 32–50, https://doi.org/10.1111/j.1600–0889.2008.00385.x, 2009.

Kandler, K., Schütz, L., Jäckel, S., Lieke, K., Emmel, C., Müller–Ebert, D., Ebert, M., Scheuvens, D., Schladitz, A., Šegvić, B., Wiedensohler, A., and Weinbruch, S.: Ground–based off–line aerosol measurements at Praia, Cape Verde, during the Saharan Mineral Dust Experiment: microphysical properties and mineralogy, Tellus B, 63, 459–474, https://doi.org/10.1111/j.1600–0889.2011.00546.x, 2011.

Khalfallah, B., Bouet, C., Labiadh, M. T., Alfaro, S. C., Bergametti, G., Marticorena, B., Lafon, S., Chevaillier, S., Féron, A., Hease, P., Tureaux, T. H. des, Sekrafi, S., Zapf, P., and Rajot, J. L.: Influence of Atmospheric Stability on the Size Distribution of the Vertical Dust Flux Measured in Eroding Conditions Over a Flat Bare Sandy Field, J. Geophys. Res: Atmos., 125, e2019JD031185, https://doi.org/10.1029/2019JD031185, 2020.

Knippertz, P. and Stuut, J.-B. W. (Eds.): Mineral Dust: A Key Player in the Earth System, Springer Netherlands, https://doi.org/10.1007/978-94-017-8978-3, 2014.

Kobayashi, H., Arao, K., Murayama, T., Iokibe, K., Koga, R., and Shiobara, M.: High–Resolution Measurement of Size Distributions of Asian Dust Using a Coulter Multisizer, J. Atmos. Oceanic Technol., 24, 194–205, https://doi.org/10.1175/JTECH1965.1, 2007.

Kok, J. F., A scaling theory for the size distribution of emitted dust aerosols suggests climate models underestimate the size of the global dust cycle. Proc Natl Acad Sci U S A 108:1016–1021, 2011

Kok, J. F., Ridley, D. A., Zhou, Q., Miller, R. L., Zhao, C., Heald, C. L., Ward, D. S., Albani, S., and Haustein, K.: Smaller desert dust cooling effect estimated from analysis of dust size and abundance, Nat. Geo. 10, 274–278, https://doi.org/10.1038/ngeo2912, 2017.

Mahowald, N., Lindsay, K., Rothenberg, D., Doney, S. C., Moore, J. K., Thornton, P., Randerson, J. T., and Jones, C. D.: Desert dust and anthropogenic aerosol interactions in the Community Climate System Model coupled-carbon-climate model, Biogeosciences, 8, 387–414, https://doi.org/10.5194/bg-8-387-2011, 2011.

Maring, H., Savoie, D. L., Izaguirre, M. A., McCormick, C., Arimoto, R., Prospero, J. M., and Pilinis, C.: Aerosol physical and optical properties and their relationship to aerosol composition in the free troposphere at Izaña, Tenerife, Canary Islands, during July 1995, J. Geophys. Res., 105, 14677–14700, https://doi.org/10.1029/2000JD900106, 2000.

Maring, H., Savoie, D. L., Izaguirre, M. A., Custals, L., and Reid, J. S.: Mineral dust aerosol size distribution change during atmospheric transport, J. Geophys. Res., 108, https://doi.org/10.1029/2002JD002536, 2003.

McConnell, C. L., Highwood, E. J., Coe, H., Formenti, P., Anderson, B., Osborne, S., Nava, S., Desboeufs, K., Chen, G., and Harrison, M. a. J.: Seasonal variations of the physical and optical characteristics of Saharan dust: Results from the Dust Outflow and Deposition to the Ocean (DODO) experiment, J. Geophys. Res., 113, https://doi.org/10.1029/2007JD009606, 2008.

Meloni, D., Junkermann, W., Sarra, A. di, Cacciani, M., Silvestri, L. D., Iorio, T. D., Estellés, V., Gómez-Amo, J. L., Pace, G., and Sferlazzo, D. M.: Altitude–resolved shortwave and longwave radiative effects of desert dust in the Mediterranean during the GAMARF campaign: Indications of a net daily cooling in the dust layer, J. Geophys. Res., 120, 3386–3407, https://doi.org/10.1002/2014JD022312, 2015.

Meng, J., Huang, Y., Leung, D. M., Li, L., Adebiyi, A. A., Ryder, C. L., Mahowald, N. M., and Kok, J. F.: Improved Parameterization for the Size Distribution of Emitted Dust Aerosols Reduces Model Underestimation of Super Coarse Dust, Geophys. Res. Lett., 49, e2021GL097287, https://doi.org/10.1029/2021GL097287, 2022.

Menut, L., Siour, G., Bessagnet, B., Couvidat, F., Journet, E., Balkanski, Y., and Desboeufs, K.: Modelling the mineralogical composition and solubility of mineral dust in the Mediterranean area with CHIMERE 2017r4, Geosci. Model Dev., 13, 2051–2071, https://doi.org/10.5194/gmd-13-2051-2020, 2020.

Müller, K., Lehmann, S., van Pinxteren, D., Gnauk, T., Niedermeier, N., Wiedensohler, A., and Herrmann, H.: Particle characterization at the Cape Verde atmospheric observatory during the 2007 RHaMBLe intensive, 10, 2709–2721, Atmos. Chem. Phys., https://doi.org/10.5194/acp–10–2709–2010, 2010.

Osborne, S. R., Johnson, B. T., Haywood, J. M., Baran, A. J., Harrison, M. a. J., and McConnell, C. L.: Physical and optical properties of mineral dust aerosol during the Dust and Biomass–burning Experiment, J. Geophys. Res., 113, https://doi.org/10.1029/2007JD009551, 2008.

Otto, S., de Reus, M., Trautmann, T., Thomas, A., Wendisch, M., and Borrmann, S.: Atmospheric radiative effects of an in situ measured Saharan dust plume and the role of large particles, Tellus B, 7, 4887–4903, https://doi.org/10.5194/acp–7–4887–2007, 2007.

Perlwitz, J.P., C. Pérez García–Pando, and R.L. Miller: Predicting the mineral composition of dust aerosols — Part 1: Representing key processes. Atmos. Chem. Phys., 15, 11593–11627, doi:10.5194/acp–15–11593–2015, 2015a.

Perlwitz, J.P., C. Pérez García–Pando, and R.L. Miller: Predicting the mineral composition of dust aerosols — Part 2: Model evaluation and identification of key processes with observations. Atmos. Chem. Phys., 15, 11629–11652, doi:10.5194/acp–15–11629–2015, 2015b.

Rajot, J. L., Formenti, P., Alfaro, S., Desboeufs, K., Chevaillier, S., Chatenet, B., Gaudichet, A., Journet, E., Marticorena, B., Triquet, S., Maman, A., Mouget, N., and Zakou, A.: AMMA dust experiment: An overview of measurements performed during the dry season special observation period (SOP0) at the Banizoumbou (Niger) supersite, J. Geophys. Res., 113, https://doi.org/10.1029/2008JD009906, 2008.

Reid, E. A., Reid, J. S., Meier, M. M., Dunlap, M. R., Cliff, S. S., Broumas, A., Perry, K., and Maring, H.: Characterization of African dust transported to Puerto Rico by individual particle and size segregated bulk analysis, J. Geophys. Res., 108, https://doi.org/10.1029/2002JD002935, 2003a.

Reid, J. S., Jonsson, H. H., Maring, H. B., Smirnov, A., Savoie, D. L., Cliff, S. S., Reid, E. A., Livingston, J. M., Meier, M. M., Dubovik, O., and Tsay, S.–C.: Comparison of size and morphological measurements of coarse mode dust particles from Africa, J. Geophys. Res., 108, https://doi.org/10.1029/2002JD002485, 2003b.

Reid, J. S., Reid, E. A., Walker, A., Piketh, S., Cliff, S., Mandoos, A. A., Tsay, S.–C., and Eck, T. F.: Dynamics of southwest Asian dust particle size characteristics with implications for global dust research, J. Geophys. Res., 113, https://doi.org/10.1029/2007JD009752, 2008.

Renard, J.–B., Dulac, F., Durand, P., Bourgeois, Q., Denjean, C., Vignelles, D., Couté, B., Jeannot, M., Verdier, N., and Mallet, M.: In situ measurements of desert dust particles above the western Mediterranean Sea with the balloon–borne Light Optical Aerosol Counter/sizer (LOAC) during the ChArMEx campaign of summer 2013, Atmos. Chem. Phys., 18, 3677–3699, https://doi.org/10.5194/acp–18–3677–2018, 2018.

de Reus, M., Dentener, F., Thomas, A., Borrmann, S., Ström, J., and Lelieveld, J.: Airborne observations of dust aerosol over the North Atlantic Ocean during ACE 2: Indications for heterogeneous ozone destruction, J. Geophys. Res., 105, 15263–15275, https://doi.org/10.1029/2000JD900164, 2000.

Rosenberg, P. D., Dean, A. R., Williams, P. I., Dorsey, J. R., Minikin, A., Pickering, M. A., and Petzold, A.: Particle sizing calibration with refractive index correction for light scattering optical particle counters and impacts upon PCASP and CDP data collected during the Fennec campaign, Atmos. Meas. Tech., 5, 1147–1163, https://doi.org/10.5194/amt–5–1147–2012, 2012.

Rosenberg, P. D., Parker, D. J., Ryder, C. L., Marsham, J. H., Garcia-Carreras, L., Dorsey, J. R., Brooks, I. M., Dean, A. R., Crosier, J., McQuaid, J. B., and Washington, R.: Quantifying particle size and turbulent scale dependence of dust flux in the Sahara using aircraft measurements, J. Geophys. Res. Atmos., 119, 7577–7598, https://doi.org/10.1002/2013JD021255, 2014.

Ryder, C. L., Highwood, E. J., Lai, T. M., Sodemann, H., and Marsham, J. H.: Impact of atmospheric transport on the evolution of microphysical and optical properties of Saharan dust, Geophys. Res. Lett., 40, 2433–2438, https://doi.org/10.1002/grl.50482, 2013a.

Ryder, C. L., Highwood, E. J., Rosenberg, P. D., Trembath, J., Brooke, J. K., Bart, M., Dean, A., Crosier, J., Dorsey, J., Brindley, H., Banks, J., Marsham, J. H., McQuaid, J. B., Sodemann, H., and Washington, R.: Optical properties of Saharan dust aerosol and contribution from the coarse mode as measured during the Fennec 2011 aircraft campaign, Atmos. Chem. Phys., 13, 303–325, https://doi.org/10.5194/acp–13–303–2013, 2013b.

Ryder, C. L., Marenco, F., Brooke, J. K., Estelles, V., Cotton, R., Formenti, P., McQuaid, J. B., Price, H. C., Liu, D., Ausset, P., Rosenberg, P. D., Taylor, J. W., Choularton, T., Bower, K., Coe, H., Gallagher, M., Crosier, J., Lloyd, G., Highwood, E. J., and Murray, B. J.: Coarse–mode mineral dust size distributions, composition and optical properties from AER–D aircraft measurements over the tropical eastern Atlantic, Atmos. Chem. Phys., 18, 17225–17257, https://doi.org/10.5194/acp–18–17225–2018, 2018.

Scanza, R. A., Mahowald, N., Ghan, S., Zender, C. S., Kok, J. F., Liu, X., Zhang, Y., and Albani, S.: Modeling dust as component minerals in the Community Atmosphere Model: development of framework and impact on radiative forcing, Atmos. Chem. Phys., 15, 537–561, https://doi.org/10.5194/acp-15-537-2015, 2015.

Schladitz, A., Müller, T., Nowak, A., Kandler, K., Lieke, K., Massling, A., and Wiedensohler, A.: In situ aerosol characterization at Cape Verde, Tellus B, 63, 531–548, https://doi.org/10.1111/j.1600–0889.2011.00569.x, 2011.

Schütz, L. and Jaenicke, R.: Particle Number and Mass Distributions above 10−4 cm Radius in Sand and Aerosol of the Sahara Desert, J. Appl. Meteor., 13, 863–870, https://doi.org/10.1175/1520–0450(1974)013<0863:PNAMDA>2.0.CO;2, 1974.

Schütz, L., Jaenicke, R. and Pietrek, H., Saharan Dust Transport over the North Atlantic Ocean. In: Péwé, T.L., Ed., Desert Dust, Geological Society of America, Boulder, Special Paper, Vol. 186, 87-100. https://doi.org/10.1130/SPE186-p87, 1981.

Shao, Y., Ishizuka, M., Mikami, M., and Leys, J. F.: Parameterization of size–resolved dust emission and validation with measurements, J. Geophys. Res., 116, https://doi.org/10.1029/2010JD014527, 2011.

Sow, M., Alfaro, S. C., Rajot, J. L., and Marticorena, B.: Size resolved dust emission fluxes measured in Niger during 3 dust storms of the AMMA experiment, Atmos. Chem., Phys., 9, 3881–3891, https://doi.org/10.5194/acp–9–3881–2009, 2009.

Struckmeier, C., Drewnick, F., Fachinger, F., Gobbi, G. P., and Borrmann, S.: Atmospheric aerosols in Rome, Italy: sources, dynamics and spatial variations during two seasons, Atmos. Chem. Phys., 16, 15277–15299, https://doi.org/10.5194/acp–16–15277–2016, 2016.

Sviridenkov, M. A., Gillette, D. A., Isakov, A. A., Sokolik, I. N., Smirnov, V. V., Belan, B. D., Pachenko, M. V., Andronova, A. V., Kolomiets, S. M., Zhukov, V. M., and Zhukovsky, D. A.: Size distributions of dust aerosol measured during the Soviet–American experiment in Tadzhikistan, 1989, Atmos. Environ., 27, 2481–2486, https://doi.org/10.1016/0960–1686(93)90019–U, 1993.

Wagner, F., Bortoli, D., Pereira, S., Costa, M. Jo., Silva, A. M., Weinzierl, B., Esselborn, M., Petzold, A., Rasp, K., Heinold, B., and Tegen, I.: Properties of dust aerosol particles transported to Portugal from the Sahara desert, Tellus B: Chemical and Physical Meteorology, 61, 297–306, https://doi.org/10.1111/j.1600–0889.2008.00393.x, 2009.

Walser, A., Sauer, D., Spanu, A., Gasteiger, J., and Weinzierl, B.: On the parametrization of optical particle counter response including instrument–induced broadening of size spectra and a self–consistent evaluation of calibration measurements, Atmos. Chem. Phys., 10, 4341–4361, https://doi.org/10.5194/amt–10–4341–2017, 2017.

Weinzierl, B., Petzold, A., Esselborn, M., Wirth, M., Rasp, K., Kandler, K., SchüTZ, L., Koepke, P., and Fiebig, M.: Airborne measurements of dust layer properties, particle size distribution and mixing state of Saharan dust during SAMUM 2006, Tellus B, 61, 96–117, https://doi.org/10.1111/j.1600–0889.2008.00392.x, 2009.

Weinzierl, B., Sauer, D., Esselborn, M., Petzold, A., Veira, A., Rose, M., Mund, S., Wirth, M., Ansmann, A., Tesche, M., Gross, S., and Freudenthaler, V.: Microphysical and optical properties of dust and tropical biomass burning aerosol layers in the Cape Verde region—an overview of the airborne in situ and lidar measurements during SAMUM–2, Tellus B, 63, 589–618, https://doi.org/10.1111/j.1600–0889.2011.00566.x, 2011.

Weinzierl, B., Ansmann, A., Prospero, J. M., Althausen, D., Benker, N., Chouza, F., Dollner, M., Farrell, D., Fomba, W. K., Freudenthaler, V., Gasteiger, J., Groß, S., Haarig, M., Heinold, B., Kandler, K., Kristensen, T. B., Mayol–Bracero, O. L., Müller, T., Reitebuch, O., Sauer, D., Schäfler, A., Schepanski, K., Spanu, A., Tegen, I., Toledano, C., and Walser, A.: The Saharan Aerosol Long–Range Transport and Aerosol–Cloud–Interaction Experiment: Overview and Selected Highlights, Bull. Amer. Meteor. Soc., 98, 1427–1451, https://doi.org/10.1175/BAMS–D–15–00142.1, 2017.

Zhao, A., Ryder, C. L., and Wilcox, L. J.: How well do the CMIP6 models simulate dust aerosols?, Atmos. Chem. Phys., 22, 2095–2119, https://doi.org/10.5194/acp-22-2095-2022, 2022.

Zhou, Y., R. C. Levy, et al. "Dust Aerosol Retrieval over the Oceans with the MODIS/VIIRS Dark Target algorithm. Part I: Dust Detection." Earth and Space Science n/a(n/a): e2020EA001221.